Journal of Structural Geology, Vol. 15, Nos 3–5, pp. 423 to 434, 1993
Printed in Great Britain

0191-8141/93 $06.00+0.00

Flow variations in power-law multilayers: implications for competence contrasts in rocks

SUSAN H. TREAGUS

Department of Geology, University of Manchester, Manchester M13 9PL, U.K.

(*Received* 16 *December* 1991; *accepted in revised form* 4 *August* 1992)

Abstract—An idealized bilaminate multilayer of alternating 'competent' and 'incompetent' layers with different proportional thicknesses is used to model theoretically the manner in which flow in rocks may vary from layer to layer during deformation. The layers are assumed to flow according to a 'power law', with stress exponent (n) of 1 (=Newtonian flow), 3 or 5, which is in accordance with current experimental data for flow in rocks. The theoretical analysis concentrates first on incompressible plane flow, and is then extended to some forms of incompressible three-dimensional flow.

Strain-rate variations from competent to incompetent layers are illustrated for two-dimensional flows on 'rheology graphs' of log stress vs log strain-rate. Three types of bulk multilayer deformation are illustrated: layer-parallel pure shearing (LPPS), layer-parallel simple shearing (LPSS) and layer-oblique straining (in different orientations). The degree of flow partitioning varies with the bulk flow, layer thicknesses, and layer n values. For all systems in plane (two-dimensional) flow, the greatest partitioning occurs for 45° bulk shortening (LPSS), and is most extreme for high n values, such that the strain-rate is virtually zero in competent members. However, for three-dimensional flows, preliminary results suggest that the value of n may play a less significant role in flow partitioning, particularly for bulk pure flattening or constrictional flows.

These theoretical flow variations provide some meaning to 'competent contrast' in rocks, and reveal possible links between relative competence and deformation history. Such flow variations in space and time may provide the driving mechanism for folding in ductile multilayered systems.

INTRODUCTION

THE geometry of naturally deformed rocks reveals the important part played by competence contrasts in the development of structures. Some of the most geometrically aesthetic geological structures, such as the folds and boudins so beautifully illustrated in John Ramsay's publications (Ramsay 1967, 1982, Ramsay & Huber 1983, 1987), are a direct result of the distinct differences in flow and material behaviour of adjacent rock layers.

To a field geologist, competence contrast is usually inferred from the degree of ductile deformation of lithologies, and from styles of structures. To a theoretician studying folding instabilities, competence contrast is equated with viscosity ratio, and so competence is an instantaneous measurement of resistance to flow. (For the varying usages and definitions of the term *competence*, see Treagus 1988.) Only if rocks flow with a constant viscosity (as Newtonian fluids) can competence contrast be considered to be a material constant for a protracted deformation, or for different deformation rates.

The question of whether ductile rocks flow as linear or non-linear fluids is of topical importance, as it affects assumptions for theoretical analyses, choice of materials for modelling, and extrapolations of laboratory data. Results drawn from decades of experimental rock deformation studies suggest that for a wide variety of rocks and experimental conditions, steady-state creep approximates to a 'power law'. For two-dimensional flows, this is commonly expressed as the Weertman relation, $\dot{e} = A \exp(-Q_c \bar{R} T)\, \sigma^n$ (Tsenn & Carter 1987) (where $\dot{e}$ is the steady-state strain rate, σ the differential stress, A a material constant, n the stress exponent, Q_c is the activation energy for creep, $\bar{R}$ the universal gas constant and T the temperature). Carter & Tsenn (1987, table 4) and Kirby & Kronenberg (1987, table 3) collate much of the data available for the above variables, for many different rock types and many different laboratory experiments.

The above relation for steady-state creep is a power law comparable with the common expression for power-law fluid flow, $\dot{e} = A\, \sigma^n$. This relation can be expressed for two-dimensional flows in terms either of shear stress and strain rates, or deviatoric normal stress and strain rate (see, e.g. Ranalli 1987, p. 75). For non-plane flows the power relation is written in terms of the second invariants of the stress and strain-rate tensors (e.g. Hobbs 1972, Fletcher 1974, Cobbold 1983).

If rocks do indeed flow according to a power law, the relationship of the viscosity contrast during a deformation, and a finite competence contrast interpreted from the contrasts in strain, could be quite complex. Since the viscosity of a power-law material changes with strain rate, any deformation of layered systems which has a non-constant flow history in the individual layers will mean that the viscosities change throughout the deformation; so in general, viscosity ratios will not remain constant.

The present paper continues my earlier theoretical analyses of variations and refraction of stress, strain-rate and finite strain in Newtonian viscous layers (Treagus 1973, 1981, 1983, 1988), and applies the same principles to layers with power-law rheology. It follows on from Cobbold's (1983) analysis of behaviour across interfaces, and from laboratory modelling which tested the

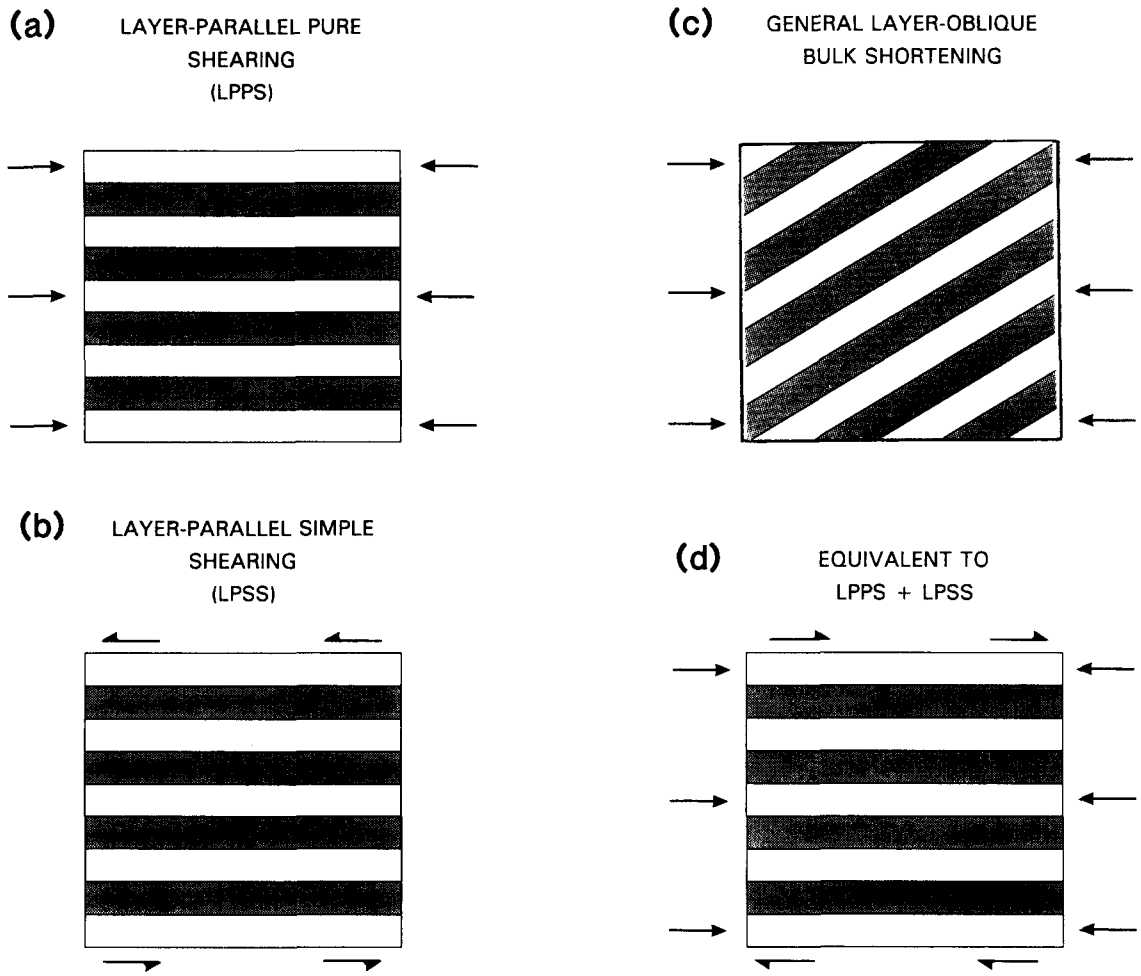

Fig. 1. Types of two-dimensional bulk flow for an idealized bilaminate multilayer. Shaded layers indicate alternating 'competent' and 'incompetent' layers, here of equal thickness ($\alpha_C = \alpha_I = 0.5$). A general layer-oblique bulk shortening given in (c) (where $\theta = 30°$) can be considered, in (d), in terms of components of LPPS and LPSS, for two-dimensional oblique-plane flows. Plane of view is the xy plane, where x is parallel to layering, y, perpendicular and z is the third dimension.

theoretical base, and measured strain variations in silicone putty layers of Newtonian and power-law-type rheology (Treagus & Sokoutis 1992). To avoid unnecessary duplication of background material, readers are referred to all these papers for the theoretical base, to Treagus (1988) for further information on competence, and to Treagus & Sokoutis (1992) for further references on the rheology of rocks.

Theoretical flow variations in ductile rocks are modelled here using an *idealized multilayer* (e.g. Fig. 1): a bilaminate system of two alternating contrasting layers, as considered by Bayly (1964), Latham (1985a) and others. The layer thickness proportions, flow properties for the component layers and layering orientation may all be considered as variables. The *bulk flow* can be considered in terms of flow in a statistically anisotropic medium (Biot 1965, p. 186, Cobbold *et al.* 1971, Cobbold 1976, Latham 1985a,b). However, in this paper I investigate the *partitioning* of a bulk flow (*sensu* Lister & Williams 1983) within the component layers of a multilayer; that is, the strain and strain-rate variations from layer to layer. Strong variations in flow between the relatively competent and incompetent components of the idealized multilayer must be expected, comparable to the finite strain variations and strain refraction found in earlier work assuming Newtonian rheology. Although the present analysis does not allow finite strain variations to be derived for power-law layers, the flow (strain-rate) variations will allow some predictions to be made about deformation histories, and the degree to which the power-law stress exponent, n, might influence degree of flow partitioning.

FLOW VARIATIONS IN A BILAMINATE MULTILAYER: THEORETICAL MODEL

Figure 1 shows examples of types of flow in idealized bilaminate multilayers, where (a) and (b) are the special deformations of layer-parallel pure shearing and layer-parallel simple shearing. Figure 1(c) shows a general layer-oblique flow, which for isovolumetric two-dimensional flows (and neglecting vorticity) can be considered in terms of components of pure and simple shearing (Fig. 1d), comparable to the analysis of finite strain as components of layer-parallel pure shear and simple shear (Treagus 1988, fig. 3).

The bilaminate multilayer is assumed to have alternating competent and incompetent layers (denoted C and I throughout the paper), deforming in bulk steady-state shortening at an angle, θ, to the layering. The flow is here assumed to be plane (two-dimensional) and incompressible. (The theoretical analysis is later applied to cases of three-dimensional flow, where layering is parallel to one principal axis of straining.) Flow in both the competent and incompetent layers follows a power law, $\dot{e} = A\ \sigma^n$, as introduced above. The alternating layers are assumed to be isotropic, and have the same value of stress exponent, n, but different A. (Values used are $n = 1$, $n = 3$ and $n = 5$.) Although it is probably an unreasonable geological assumption that competent and incompetent layers have equal n values, it is convenient for the present analysis in order to find simple solutions to the equations.

The requirements of compatibility and continuity for the multilayer in flow are equivalent to those in the earlier stress and strain refraction analyses (see Treagus 1973, 1981, 1983, 1988, Cobbold 1983): equal layer-parallel normal straining and equal layer-parallel shear stress. In addition, for the present multilayer approach, the sum of individual layer-parallel shear strain rates determines the bulk layer-parallel shear strain rate as for anisotropy theory (Biot 1965, p. 432).

Appendix 1 presents a detailed algebraic derivation of flow variations in the idealized power-law multilayer, following the above assumptions and theoretical requirements. The three general equations necessary to derive solutions are summarized below, and results and examples given in the following section of the paper.

Summary of equations for two-dimensional flow variations, from Appendix 1

Use θ, for the orientation of principal bulk shortening to the layering, and θ_C and θ_I for the competent and incompetent layers, respectively. Normalize all the principal strain rates as factors of the bulk principal (elongating) strain-rate:

$$\text{e.g. } \varepsilon_C = \dot{e}_{1(C)}/\dot{e}_{1(\text{bulk})}.$$

Use α_C and α_I to denote thickness proportions of competent and incompetent layers, respectively (as for anisotropy theory), where $\alpha_C + \alpha_I = 1$. The viscosity ratio (μ_C/μ_I) is termed M, where μ_C and μ_I are the viscosity terms for competent and incompetent layers, respectively. M will be determined as a function of R, where R is the viscosity ratio for layer-parallel pure shearing.

From Appendix 1 (equation A16), for $0 < \theta < 45°$ or $45 < \theta < 90°$,

$$M \approx R[1 + \tan^2 2\theta/\alpha_I^2]^{(n-1)/2n}. \quad (1)$$

For equal thickness layers ($\alpha_C = \alpha_I = 0.5$),

$$M \approx R[1 + 4\tan^2 2\theta]^{(n-1)/2n}.$$

For $\theta = 45°$, or layer-parallel simple shearing, $M = R^n$, regardless of relative thicknesses.

From (A9)

$$\tan 2\theta_C = \tan 2\theta/(\alpha_C + M\alpha_I) \quad (2a)$$

$$\tan 2\theta_I = M \tan 2\theta/(\alpha_C + M\alpha_I). \quad (2b)$$

For equal thickness layers ($\alpha_C = \alpha_I = 0.5$),

$$\tan 2\theta_C = 2\tan 2\theta/(1 + M),$$

$$\tan 2\theta_I = 2M \tan 2\theta/(1 + M).$$

From (A3)

$$\varepsilon_C = \cos 2\theta/\cos 2\theta_C \quad (3a)$$

$$\varepsilon_I = \cos 2\theta/\cos 2\theta_I. \quad (3b)$$

For $\theta = 45°$, $\varepsilon_C/\varepsilon_I = 1/M$, and

$$\varepsilon_C = 1/(\alpha_C + M\alpha_I)$$

$$\varepsilon_I = M/(\alpha_C + M\alpha_I).$$

Equations (1)–(3) provide the method of determining the properties of two-dimensional flow in a bilaminate multilayer. The following sections provide some examples of results obtained using this algebra.

TWO-DIMENSIONAL FLOW VARIATIONS IN A BILAMINATE MULTILAYER: RESULTS AND EXAMPLES

The rheology graph

A useful way to illustrate the relationship between flow variations and rheology for different materials can be made (for plane flows) on a log $\dot{e}$ vs log σ graph, here called a *rheology graph*. This graph has been used to represent rheology of model materials like silicone putties, plasticines and waxes (e.g. Cobbold 1975, McClay 1976, Dixon & Summers 1985, 1986, Weijermars & Schmeling 1986, Sokoutis 1987, Mancktelow 1988). Treagus & Sokoutis (1992) have recently used such graphs to represent flow variations across rheological boundaries for their laboratory models.

The log stress vs log strain-rate graphs used in this paper are drawn in terms of maximum shear stress and strain rates (τ and $\dot{\gamma}$), but the diagrams are interchangeable with maximum differential stress vs longitudinal strain-rate (σ and $\dot{e}$). On both types of graph, if axes are drawn to the same scale, Newtonian materials ($n = 1$) follow 45° diagonals, and power-law materials straight lines whose gradients are $1/n$.

This type of graph allows the relationships between bulk multilayer flows and individual layer flows to be represented, and important principles illustrated immediately. Results of flow variations for layers with $n = 1$, 3 or 5, and particular thickness proportions, derived algebraically from equations (1)–(3), can be readily compared, graphically.

Layer-parallel pure shearing, and layer-parallel simple shearing

A rheology graph clearly illustrates the differences of flow for layer-parallel pure shearing (LPPS) and simple

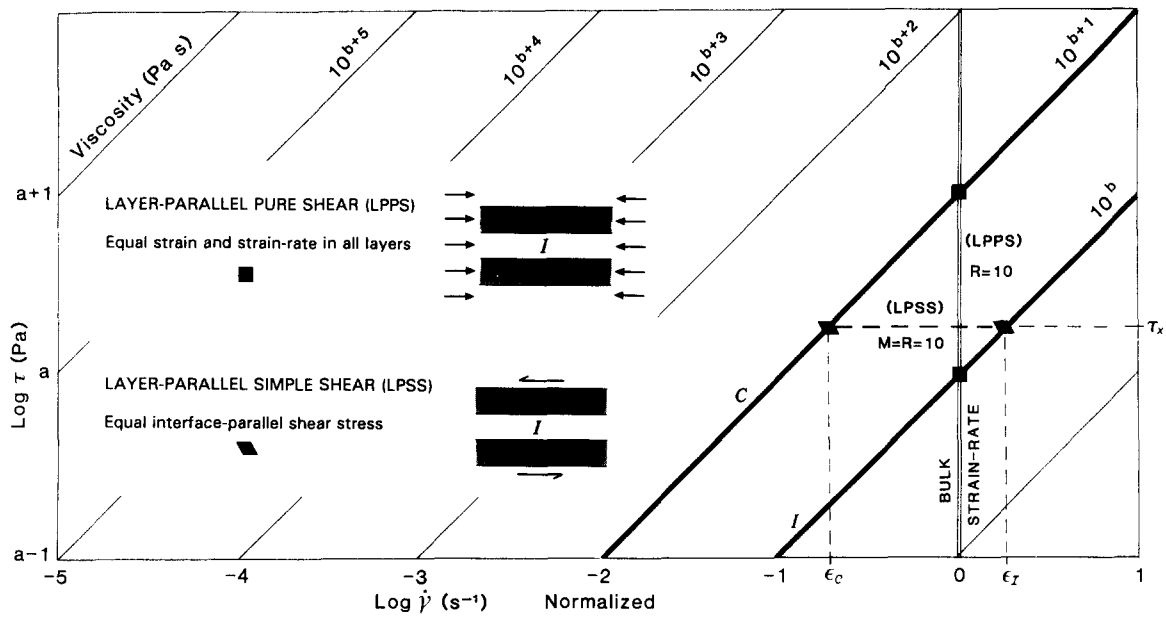

Fig. 2. Rheology graph for two imaginary Newtonian materials (C, I) with viscosity ratio of $R = 10$, for deformations of layer-parallel pure shearing (LPPS) and layer-parallel simple shearing (LPSS) for the idealized multilayers (inset, and Fig. 1a & b). The stress and viscosity scales are arbitrary (relative), and the strain-rate scale is shown relative to the bulk principal strain-rate (i.e. normalized; log ε). Squares indicate layer strain-rates for LPPS, and diamonds for LPSS. Vorticity is not represented on the diagram. See inset and text for explanation. For an alternative dimensionless diagram, the axes would be log ($\dot{\gamma}$/s^{-1}) and log (τ/Pa).

shearing (LPPS) of multilayered systems. These two special deformations (Figs. 1a&b) are illustrated for a bilaminate of equal layer thickness proportions, in Figs. 2 and 3, for Newtonian and power-law ($n = 3$ or 5) multilayers, and $R = 10$.

It is apparent that for LPPS, the strain-rate is required to be the same in the two layers (homogeneous flow), and so flow 'tie-lines' between competent and incompetent layers are ordinate-parallel. For LPSS, the tie-lines are abscissa-parallel (constant stress), because of the requirement of equal layer-parallel shear stress, which for this deformation means constant stress. Thus it follows that for LPSS, the strain-rates must be different (by the inverse viscosity ratio). The partitioning of flow between competent and incompetent members is indicated by values of ε_C and ε_I in Fig. 2 (Newtonian) and Table 1 (all), derived algebraically as given above. It is clear, from comparison of Figs. 2 and 3(b), that there is greater flow partitioning between the layers (C, I), at higher n.

Figures 2 and 3 illustrate that the viscosity ratio, M, is not equivalent to R, except for the Newtonian example. The relationship, $M = R^n$, for LPSS is graphically evident. It is also evident that competent and incompetent layers with the same n value (represented by parallel lines) have viscosity ratios for pure shearing and simple shearing which are independent of strain-rate. However, for two layers with different n (non-parallel C and I lines; not illustrated), M is also dependent on strain-rate, and materials can even exchange relative competence, when their representing lines cross over (see Treagus & Sokoutis 1992, fig. 12b).

General layer-oblique bulk flows

Equations (1)–(3) (also Appendix 1) allow flow variations to be calculated, and principal strain-rate orientations determined, for a bilaminate of any thickness proportion and power-law flow properties, with the restriction that both component layers have the same stress exponent, n, as noted earlier. The main set of examples presented here are the equal-thickness layers and $R = 10$. Comparisons are made for different layer orientations, and for $n = 1$, 3 and 5. Other thickness proportions are investigated later.

Table 1. Numerical values of flow variations for bulk plane straining, for the examples illustrated in Figs. 2–6. All multilayers have equal-thickness competent and incompetent layers, as in Fig. 1, and $R = 10$. θ is the orientation of bulk shortening to layering, M is the shear viscosity ratio, ε_C and ε_I are normalized principal extensional flows, and θ_C and θ_I orientations of principal shortening flows (C = competent, I = incompetent). LPPS = layer-parallel pure shearing; LPSS = layer-parallel simple shearing. For $\theta = 60°$, the M, ε_C values are equivalent to the 30° case, and θ_C and θ_I angles are complementary

$R = 10$	θ	M	ε_C	ε_I	θ_C	θ_I
$n = 1$						
LPPS	0	10	1	1	0	0
	30°	10	0.52	1.65	8.73°	36.2°
LPSS	45°	10	0.18	1.82	45°	45°
$n = 3$						
LPPS	0	10	1	1	0	0
	30°	23.5	0.5	1.73	4.02°	36.62
LPSS	45°	10^3	0.002	2.0	45°	45°
$n = 5$						
LPPS	0	10	1	1	0	0
	30°	27.9	0.50	1.75	3.42°	36.68°
LPSS	45°	10^5	0.00002	2.0	45°	45°

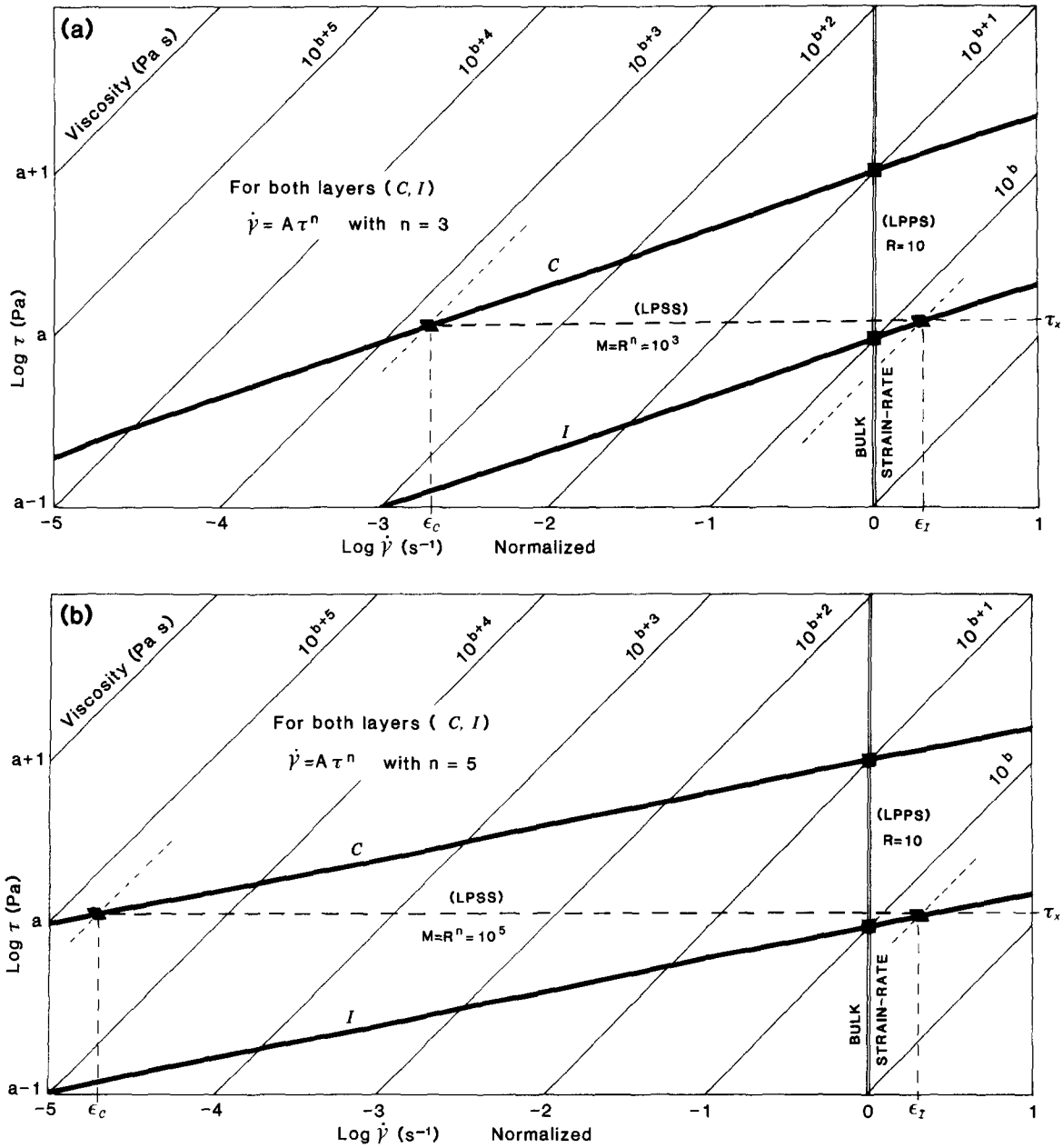

Fig. 3. Rheology graphs, as Fig. 2, but here representing an equal-thickness bilaminate with both layers in power-law flow and with equal stress exponent: (a) $n = 3$; (b) $n = 5$. The viscosity ratio for layer-parallel pure shearing (LPSS) (R) is 10. All symbols and abbreviations as in Fig. 2. Further explanation in the text.

Figure 4 shows normalized flows (ε) for the equal-thickness *Newtonian multilayer* (also Fig. 2), for bulk shortening orientations in 10° intervals of θ, from 0 to 90°. The 45°-shortening position can be considered equivalent to layer-parallel simple shearing (LPSS in Fig. 2), for instantaneous flow, and neglecting vorticity. Complementary angles of layer orientation, such as 30° and 60°, yield the same results for normalized strain-rates (Fig. 4), and complementary angular results. Figure 4 gives values of ε for 30° (60°), compared to values for 0, 45 and 90° (also Table 1). In the competent layers, flow is partitioned to roughly half of the bulk flow at 30°; it is about a fifth at 45°. In the incompetent layers at 45°, flow is partitioned up to almost twice the bulk rate, and the difference between 30 and 45° is less distinct.

Figure 5 shows flow variations for equal thickness *power-law multilayers* with $R = 10$, and (a) $n = 3$ or (b) $n = 5$, for 0, 30, 45, 60 and 90° shortening orientation to layering. Numerical values of M, ε_C, ε_I, θ_C, θ_I are given in Table 1. Note that the viscosity ratio (M) for 30° (or 60°), computed according to equation (1), is 23 for $n = 3$, and 30 for $n = 5$. Although considerably more than the value of 10 for layer-parallel shortening, these are magnitudes less than the value of 10^3 for $n = 3$, and 10^5 for $n = 5$, for layer-parallel simple shearing (45°). Thus, the changes in viscosity ratios and flow partitioning as layer orientations go from 30 to 45°, or 45 to 60°, are dramatic. For the $n = 5$ example (Fig. 5b), the decrease in ε_C from 0 to 45° is more than four orders of magnitude, which in effect means that flow virtually stops in the competent layers, at 45°. In contrast, the flow in the incompetent layers is almost the same for 30

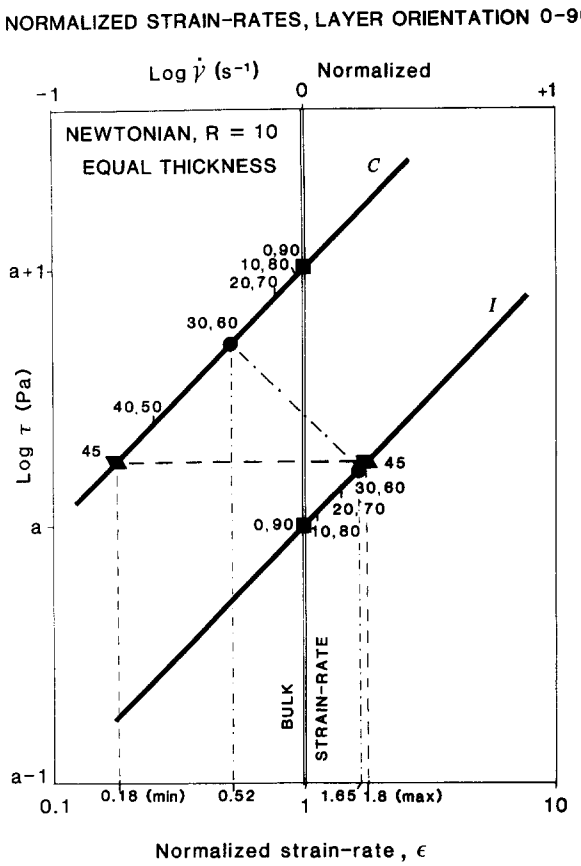

Fig. 4. Flow variations for oblique multilayer shortening, such as Fig. 1(c), represented on a rheology graph (cf. Fig. 2) for equal-thickness Newtonian multilayers. Pairs of numbers (e.g. 0, 90; 30, 60) indicate orientation of bulk shortening to layering θ (degrees); complementary angles have numerically equivalent strain-rates. Numerical values of normalized principal strain-rates (ε) are given for θ = 0 (90), 30 (60), and 45°; see also Table 1.

Table 2. Effect of competent and incompetent layer thickness proportions in a multilayer on the flow variations. α_C = 0.5 values are the equal-thickness examples in Figs. 1–6. (a) θ = 45°, equivalent to layer-parallel simple shearing, for five thickness proportions; n = 1 (Newtonian) is illustrated in Fig. 7. Note that for n = 3 and 5, ε_I is almost exactly equal to $1/\alpha_I$. (b) θ = 30° for three thickness proportions. For θ = 60°, all angles are complementary to these 30° results, and other variables the same. See text for full discussion

(a)	R = 10	θ = 45°			
α_C	α_I		ε_C	ε_I	$\theta_C = \theta_I$ = 45°
n = 1	M = 10				
0.9	0.1		0.52	5.52	
0.67	0.33		0.25	2.5	
0.5	0.5		0.18	1.18	
0.33	0.67		0.15	1.47	
0.1	0.9		0.11	1.11	
n = 3	M = 10^3				
0.9	0.1		0.01	9.91	
0.67	0.33		0.003	3.02	
0.5	0.5		0.002	1.20	
0.33	0.67		0.0015	1.49	
0.1	0.9		0.001	1.11	
n = 5	M = 10^5				
0.9	0.1		0.0001	10	
0.67	0.33		0.0000	3.03	
0.5	0.5		0.0000	2.0	
0.33	0.67		0.0000	1.49	
0.1	0.9		0.0000	1.11	

(b)	R = 10	θ = 30°				
α_C	α_I	M	ε_C	ε_I	θ_C	θ_I
n = 1						
0.9	0.1	10	0.68	4.48	21.2°	41.8°
0.5	0.5	10	0.52	1.65	8.73°	36.2°
0.1	0.9	10	0.51	1.09	5.39°	31.4°
n = 3						
0.9	0.1	67	0.51	7.17	6.4°	43°
0.5	0.5	23.5	0.5	1.73	4.02°	36.62°
0.1	0.9	16.7	0.61	1.08	3.26°	31.2°
n = 5						
0.9	0.1	98	0.51	7.96	4.6°	43.2°
0.5	0.5	27.9	0.50	1.75	3.42°	36.68°
0.1	0.9	18.6	0.50	1.08	2.94°	31.2°

and 45°; close to twice the bulk flow. In the incompetent layers the differences in normalized flow for different n (Table 1; ε_I) are very slight.

Such small flow fluctuations in incompetent layers, and less sensitivity to n, compared with orders-of-magnitude variations in the competent layers, are likely to be of importance in the deformation history of multilayers, whether they fold or not. The results here suggest that incompetent layers in a multilayer will be likely to flow more closely to 'steady state', whereas competent layers could experience rapid decelerations and accelerations of flow, especially where layer rotations accompany bulk flow.

Orientations of principal strain-rates: strain-rate refraction

Accompanying the partitioning of flow from layer to layer in the bilaminate multilayer are changes in principal strain-rate orientation, given by equation (2). For the Newtonian example, these are equivalent to the stress (or strain-rate) refraction relationships of earlier work (Treagus 1973, 1981).

Orientations of principal straining are given in Fig. 6. Clearly, no refraction occurs at 0° or 90° (homogeneous pure shearing), and 45° (heterogeneous simple shearing). For the Newtonian example, the maximum incremental strain refraction occurs for layers in the 30–40° (or 50–60°) orientation range. The values for the n = 2, 3 or 5 multilayers, for 30 or 60° layering orientation (Fig. 6, Table 1), show almost the same principal strain-rate orientation in incompetent layers as the Newtonian case, confirming relative insensitivity to n. However, in the competent layers the principal directions are more noticeably different, for different n, and more nearly layer-parallel at higher n. This could be anticipated from the flow variation results discussed above.

Effect of layer thickness

Figure 7 illustrates the effect of varying layer thickness proportions, α_C and α_I, on flow partitioning in the Newtonian multilayer at 45° to bulk shortening (or LPSS): this is the situation where the normalized principal flows are the minimum values for competent members, and the maximum for incompetent (as arrowed in Fig. 7). It is apparent that the greatest differences from the bulk flow (given by ε values) occur in the thinnest

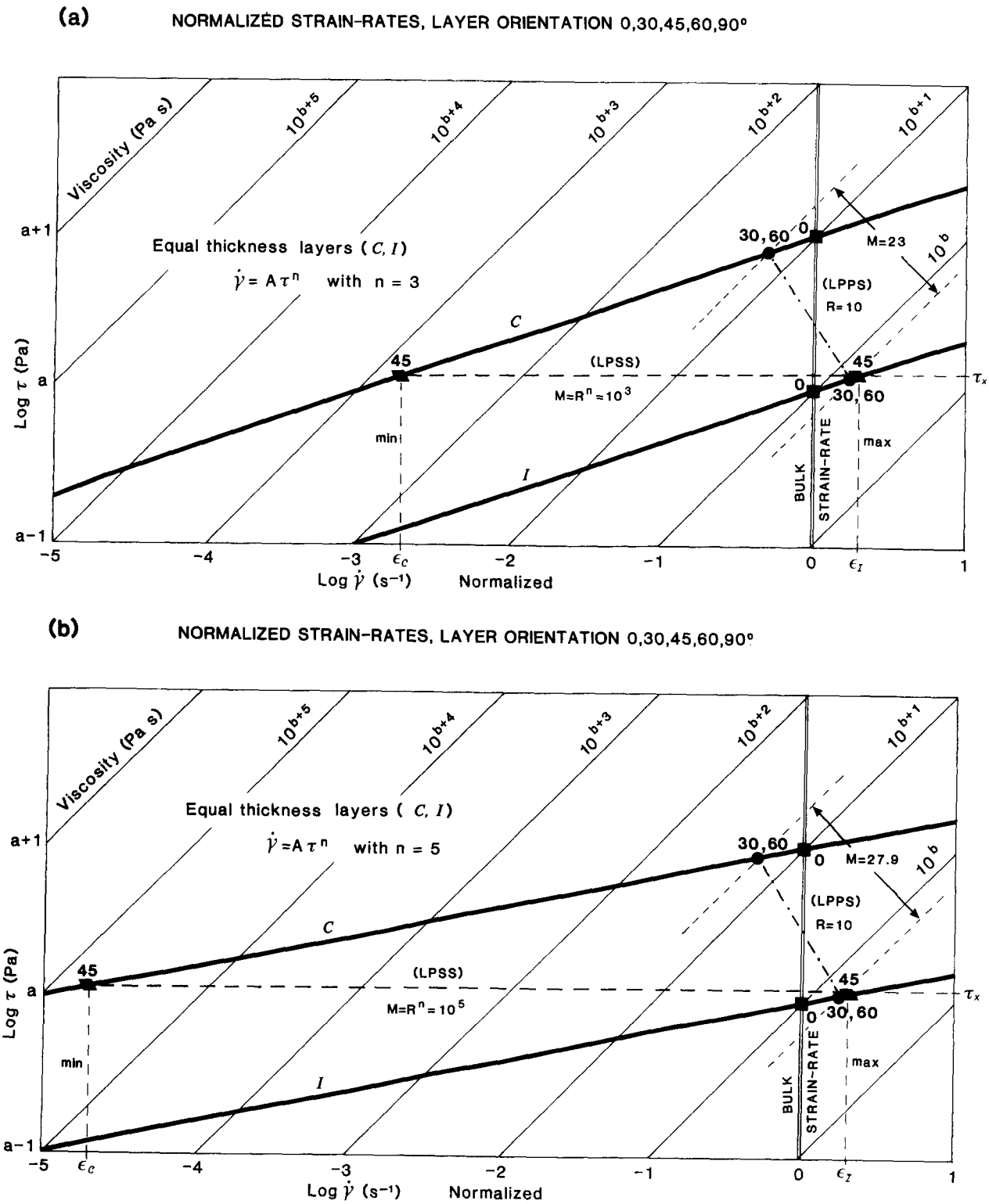

Fig. 5. Flow variations for oblique multilayer shortening such as Fig. 1 (c), represented on a rheology graph for two equal-thickness power-law multilayers: (a) $n = 3$ (as Fig. 3a); (b) $n = 5$ (as Fig. 3b). Flow partitioning is represented for $\theta = 30$ (60), and 45°. Numerical values are given in Table 1.

layers (see 0.1 positions). Conversely, the major-thickness components are closer to the bulk flow, though less so for thick competent layers; even where $\alpha_C = 0.9$, normalized flow in competent members is only half the bulk rate.

Table 2 compares the results of flow for different thicknesses of layers, for the $n = 1$, 3 and 5 multilayers with unequal layer thicknesses. Values are given for 45°-shortening (LPSS), which include the data in Fig. 7, and for 30°- or 60°-shortening. Results for 45° (Table 2a) show that $\varepsilon_I \simeq 1/\alpha_I$, for $n = 3$ or more. Hence, for a thin incompetent layer such as $\alpha_I = 0.1$, ε_I approaches 10

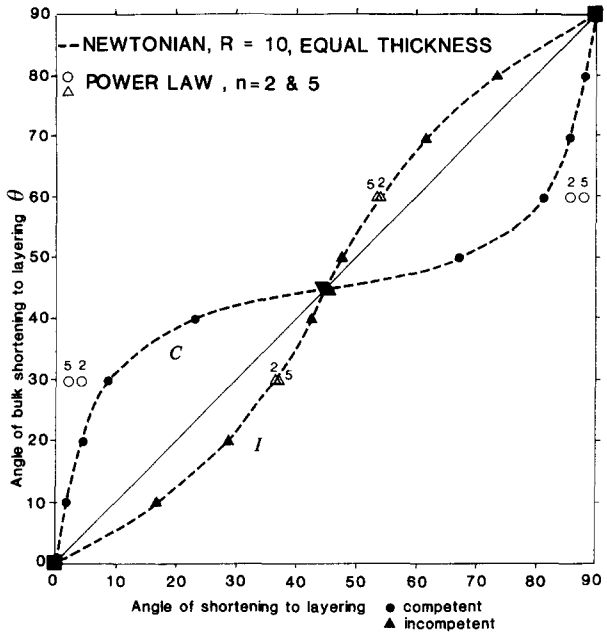

Fig. 6. Orientations of principal shortening in competent (C) and incompetent (I) layers (θ_C, θ_I), for the Newtonian multilayer examples represented in Fig. 4. Values are also given for power-law multilayers with $n = 2$ and 5, for $\theta = 30$ and 60°. For $n = 3$, see Table 1.

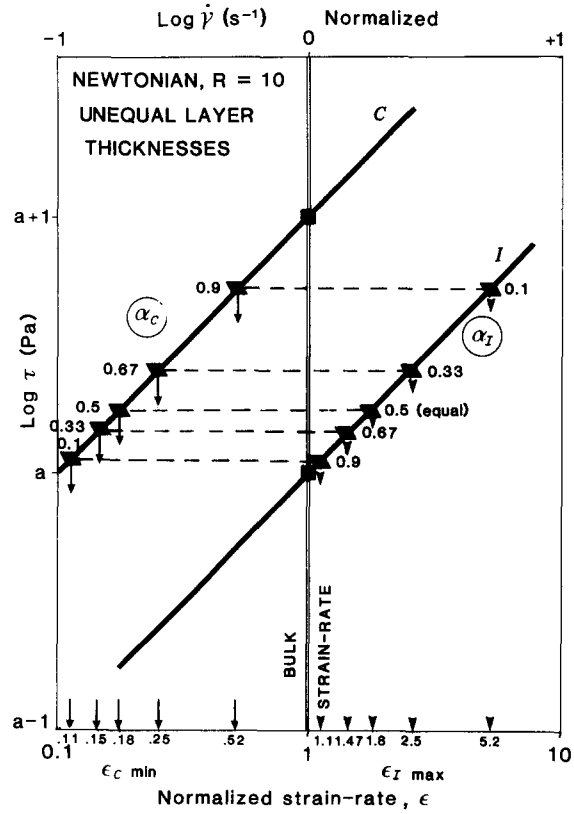

Fig. 7. Effect of layer thickness proportions, α_C (competent) and α_I (incompetent), on flow partitioning for the Newtonian multilayer ($R = 10$) in 45° shortening, or LPSS (compare with Fig. 4). Numerical values of normalized principal flows (ϵ_C and ϵ_I) are given by arrows, and marked min. and max. to indicate that for a particular multilayer, these values at 45° indicate the minimum flow for the competent members, and the maximum for the incompetent. Comparable values for $n = 3$ and $n = 5$ multilayers are given in Table 2.

times the bulk strain-rate. For similarly thin competent layers, flow is virtually zero, and approaches the bulk state in the thick incompetent members. Because flow is increasingly partitioned for increasing n, the flow in the competent layers can be virtually neglected for high n, all the flow being partitioned into the incompetent members.

Results for 30° (in Table 2b) reveal surprisingly little variation in flow rates in competent layers, either with layer thickness or with n value. (Recall that for $\theta = 45°$, $M = R^n$, regardless of thicknesses.) Computed values of M for 30° or 60° (in Table 2) show distinct variations with thickness; M is highest when the incompetent layers are very thin, and lowest when the competent components are thinnest. Even for the thinnest incompetent layer ($\alpha_I = 0.1$), and the cases used of $n = 3$ or 5, the approximation used in solution of M (Appendix 1, 4) is valid. The orientations of principal strain-rates in these 30 or 60° examples (θ_C, θ_I; Table 2) show very little variation in incompetent layers, for different n values, as noted earlier. The variations for competent layers are more marked between $n = 1$ and 3, than between 3 and 5.

The results described for 45°-shortening, or layer-parallel simple shearing, illustrate the maximum possible flow partitioning for a particular multilayer. It is apparent that most of the bulk flow in these multilayers is carried by the incompetent members, particularly for the higher n systems. In theory, for incompetent layers approaching negligible thickness, their normalized strain-rates could approach infinity. This provides a possible model for layer-parallel slip in ductile systems: a multilayer consisting of repeated layers of one material component, separated by lubricated interfaces modelled as negligibly thin incompetent layers.

THREE-DIMENSIONAL FLOW IN A BILAMINATE MULTILAYER

Where flow is three-dimensional, and includes flow perpendicular to the plane of view in Fig. 1, the algebra becomes more complex because the power law is written in terms of second invariants of stress and strain-rate (not just a single maximum strain-rate, $\dot{e}_1$).

Only the case in which one principal strain-rate is parallel to layering, in the third (z) dimension perpendicular to the page in Fig. 1(c), will be considered in this paper. This system has formerly been termed "two-dimensionally oblique" (Treagus 1981, 1988). The mathematics for fully oblique three-dimensional flow in power-law multilayers, comparable to the treatment in Treagus (1981) for Newtonian systems, is too complex for this present approach.

The algebra for three-dimensional flows in two-dimensionally oblique systems is given in Appendix 2, presented in companionship with the case of plane flows given in Appendix 1. Only a few examples have been computed so far (Table 3), and so the results and conclusions drawn are somewhat tentative.

Table 3. Flow variations for bulk three-dimensional straining. Numerical results are given for the two special cases of bulk pure flattening and bulk pure constriction, for equal-thickness layers at 30° or 45° to bulk shortening ($\dot{e}_3$, in the xy plane, as Fig. 1c). For $\theta = 60°$, all angles are complementary to the 30° results, and other variables the same. See notes (* and †) about orientations of principal straining axes, indicating switches in axes from competent to incompetent layers

n	θ (°)	M	ε_C	ε_I	θ_C (°)	θ_I (°)
$R = 10$		Bulk pure flattening			$E = 1$	
1	45	10	−0.23*	2.23	45	45
3	45	23.5	−0.38*	2.38	45	45
5	45	27.9	−0.40*	2.40	45	45
Limiting values		36.06	−0.42*	2.42	45	45
1	30	10	0.29*	1.98	8.74	36.19
3	30	18.3	0.26*	2.07	5.04	36.53
5	30	20.7	0.26*	2.09	4.54	36.58
Limiting values		24.8	0.26*	2.11	3.82	36.64
$R = 10$		Bulk pure constriction			$E = -0.5$	
1	45	10	0.39	1.61	45†	45
3	45	23.5	0.31	1.69	45†	45
5	45	27.9	0.30	1.70	45†	45
Limiting values		36.06	0.29	1.71	45†	45
1	30	10	0.64	1.49	8.74†	36.19
3	30	18.3	0.63	1.54	5.04†	36.53
5	30	20.7	0.63	1.54	4.54†	36.58
Limiting values		24.8	0.63	1.55	3.82†	36.64

* For competent layers, normalized principal flows (ε_C) refer to $\dot{e}_2$ values, as $\dot{e}_1$ axes are parallel to $\dot{e}_z$ (so true $\varepsilon_C = E$). For incompetent layers, $\dot{e}_2$ are parallel to $\dot{e}_z$.

† For competent layers, angles of shortening (θ_C) refer to $\dot{e}_2$ axes, as $\dot{e}_3$ axes are parallel to $\dot{e}_z$. For incompetent layers, $\dot{e}_2$ are parallel to $\dot{e}_z$.

Summary of equations derived in Appendix 2

Using the same definitions of variables as previously, plus defining $E = \dot{e}_2/\dot{e}_1$ (bulk), and $F = E^2/(2 + E)^2$, the necessary equations are

$$M = R[1 + \sin^2 2\theta/\{\alpha_I^2 (\cos^2 2\theta + 3F\}]^{(n-1)/2n} \quad (4)$$

$$\tan 2\theta_C = \tan 2\theta/(\alpha_C + M\alpha_I) \quad (5a)$$

$$\tan 2\theta_I = M \tan 2\theta/(\alpha_C + M\alpha_I) \quad (5b)$$

and

$$\varepsilon_C = \tfrac{1}{2}[(2 + E)\cos 2\theta/\cos 2\theta_C - E] \quad (6a)$$

$$\varepsilon_I = \tfrac{1}{2}[(2+E)\cos 2\theta/\cos 2\theta_I - E]. \quad (6b)$$

For $\theta = 45°$

$$\varepsilon_C = \tfrac{1}{2}[(2 + E)/(\alpha_C + M\alpha_I) - E]$$

$$\varepsilon_I = \tfrac{1}{2}[M(2 + E)/(\alpha_C + M\alpha_I) - E].$$

Results and examples

A few examples of results obtained from the above algebra are given in Table 3. Attention will be focused in particular on examples of equal-thickness bilaminate multilayers in bulk flattening or constrictional flow.

It is interesting to compare results for 45° layer orientations with those derived earlier for plane flows. The relationship, $M = R^n$, for $\theta = 45°$, or layer-parallel simple shearing, is only found for plane (two-dimensional) flows. Such extreme variations of M with θ, particularly at higher n, are not found for the pure flattening or constrictional flows. It is apparent in Table 3 that M values are higher for $\theta = 45°$ than for 30°, but only by about 50%.

For three-dimensional flows, the expression for M (equation 4) has a limiting value, for any set of α_C, θ, etc., because at high n, the exponent term, $\{(n-1)/2n\}$, approaches 1/2. So the orders-of-magnitude changes in M from R to R^n, found for plane flow at significant values of n (e.g. $n = 5$; Fig. 3b), are not reached in pure flattening or constriction (see limiting values, Table 3). It seems as if the power-law effect is suppressed, and such multilayers differ far less significantly from Newtonian layers (with equivalent R) than they do in plane flows. This is confirmed by only slight variations in ε values, for increasing n (Table 3).

An important result for the flattening and constrictional examples are the switches in principal straining axes from competent to incompetent layers, as indicated in Table 3 by which principal axes are parallel to $\dot{e}_z$. These are comparable to the interchanges of finite strain axes in three-dimensional strain refraction (Treagus 1983). Thus, switches in straining directions between competent and incompetent layers are likely to be found for other types of bulk three-dimensional flows, particularly if close to flattening or constriction. This remains to be demonstrated with further studies.

APPROXIMATIONS AND CONCLUSIONS

Flow partitioning in multilayers, in two dimensions

(1) Most of the bulk multilayer flow becomes partitioned in the incompetent layers, for layer orientations of 30–60° (θ) to bulk shortening.

(2) Maximum partitioning occurs at the 45° orientation to shortening, or layer-parallel simple shearing (LPSS). Partitioning is most marked at higher values of the power-law exponent, n.

(3) Flow in competent layers is highly sensitive to θ and to n. Minimum flow is always at 45°, and becomes negligible with high n.

(4) For incompetent layers, the values and orientations of principal strain rates are relatively insensitive to n.

(5) The maximum normalized flow for the incompetent layers can be approximated (except for greatly unequal layer thicknesses) to $\varepsilon_I \approx 1/\alpha_I$ (i.e. insensitive to R and n). So for equal-thickness layers, $\varepsilon_I \approx 2$; i.e. twice the bulk flow. Thus, the strain-rate in incompetent layers in an equal-thickness bilaminate will only vary between one and two times the bulk rate.

Three-dimensional flow variations

(1) For non-plane flows there is a more complex relationship between flow, viscosity ratio and layer orientation than for plane flows.

(2) Preliminary results show a lower degree of flow partitioning for bulk flattening and constrictional flows than for plane straining.

(3) The value of n does not appear to have a significant effect on the partitioning of flow, for bulk flattening or constriction. This leads to the tentative conclusion that for these special deformations, power-law multilayers may be validly approximated to Newtonian systems.

Geological conclusions: implications for the geometry of deformed rocks

(1) If rocks in ductile deformation flow as power-law fluids, the viscosity or competence contrast can be expected to vary during deformation.

(2) Multilayered rocks which are not in homogeneous layer-parallel shortening should have undergone a complex history of flow partitioning between relatively competent and incompetent layers, during a finite deformation.

(3) Rocks undergoing layer-parallel simple shear should have strongly partitioned deformation. If flow is according to the power law (e.g. $n = 3$ or 5), virtually all the multilayer deformation should be accommodated within the incompetent layers.

(4) The incompetent lithologies will probably have deformed in rough approximation to steady-state non-coaxial flow (simple-shear dominated). The competent lithologies will probably have experienced fluctuatingly weak flow, close to coaxial, and close to layer-parallel or layer-perpendicular.

(5) During a deformation, flow variations in space between adjacent layers, and in time within any particular layer, will provide important controls on folding within multilayered systems, particularly within fold-limb packages.

(6) Though the theoretical results are based on steady strain-rates, and so are probably not directly applicable to folding, they do tend to reinforce classical fold-strain models: i.e. tangential longitudinal strain with negligible limb strain in relatively competent layers; flexural flow or layer-parallel shear for incompetent layers; and homogeneous strain only for bulk layer-parallel straining, or materials with no effective viscosity ratio.

Acknowledgements—I should like to thank John Ramsay and all the organizers of the "Ramsay Meeting" at ETH, Zürich, for providing the opportunity for me to present this work to celebrate John's 60th birthday. The helpful comments from the reviewers, Peter Cobbold and Ray Fletcher, are much appreciated.

REFERENCES

Bayly, M. B. 1964. A theory of similar folding in viscous materials. *Am. J. Sci.* **262**, 753–766.

Biot, M. A. 1965. *Mechanics of Incremental Deformations*. John Wiley & Sons, New York.

Carter, N. L. & Tsenn, M. C. 1987. Flow properties of continental lithosphere. *Tectonophysics* **136**, 27–63.

Cobbold, P. R. 1975. Fold propagation in a single embedded layer. *Tectonophysics* **27**, 333–351.

Cobbold, P. R. 1976. Mechanical effects of anisotropy during large finite deformations. *Bull. Soc. géol. Fr.* **18**, 1497–1510.

Cobbold, P. R. 1983. Kinematic and mechanical continuity at a coherent interface. *J. Struct. Geol.* **5**, 341–349.

Cobbold, P. R., Cosgrove, J. W. & Summers, J. M. 1971. Development of internal structures in deformed anisotropic rocks. *Tectonophysics* **12**, 23–53.

Dixon, J. M. & Summers, J. M. 1985. Recent developments in centrifuge modelling of tectonic processes: equipment, model construction techniques and rheology of model materials. *J. Struct. Geol.* **7**, 83–102.

Dixon, J. M. & Summers, J. M. 1986. Another word on the rheology of silicone putty: Bingham. *J. Struct. Geol.* **8**, 593–595.

Fletcher, R. C. 1974. Wavelength selection in the folding of a single layer with power-law rheology. *Am J. Sci.* **274**, 1029–1043.

Hobbs, B. E. 1972. Deformation of non-Newtonian materials in simple shear. In: *Flow and Fracture of Rocks* (edited by Heard, H. C., Borg, I. Y., Carter, N. L. & Raleigh, C. B.). *Am. Geophys. Un. Geophys. Monogr.* **16**, 243–258.

Kirby, S. H. & Kronenberg, A. K. 1987. Rheology of the lithosphere: selected topics. *Rev. Geophys.* **25**, 1219–1244.

Latham, J.-P. 1985a. The influence of nonlinear material properties and resistance to bending on the development of internal structures. *J. Struct. Geol.* **7**, 225–236.

Latham, J.-P. 1985b. A numerical investigation and geological discussion of the relationship between folding, kinking and faulting. *J. Struct. Geol.* **7**, 237–249.

Lister, G. S. & Williams, P. F. 1983. The partitioning of deformation in flowing rock masses. *Tectonophysics* **92**, 1–33.

Mancktelow, N. S. 1988. The rheology of paraffin wax and its usefulness as an analogue for rocks. *Bull geol. Instn. Univ. Uppsala* **14**, 181–193.

McClay, K. R. 1976. The rheology of plasticine. *Tectonophysics* **33**, T7–T15.

Ramsay, J. G. 1967. *Folding and Fracturing of Rocks*. McGraw-Hill, New York.

Ramsay, J. G. 1982. Rock ductility and its influence on the development of tectonic structures in mountain belts. In: *Mountain Building Processes* (edited by Hsu, K. J.). Academic Press, London, 111–127.

Ramsay, J. G. & Huber, M. I. 1983. *The Techniques of Modern Structural Geology, Volume* 1: *Strain Analysis*. Academic Press, London.

Ramsay, J. G. & Huber, M. I. 1987. *The Techniques of Modern Structural Geology, Volume* 2: *Folds and Fractures*. Academic Press, London.

Ranalli, G. 1987. *Rheology of the Earth*. Allen Unwin, London.

Sokoutis, D. 1987. Finite strain effects in experimental mullions. *J. Struct. Geol.* **9**, 233–242.

Treagus, S. H. 1973. Buckling stability of a viscous single-layer system oblique to the principal compression. *Tectonophysics* **19**, 271–289.

Treagus, S. H. 1981. A theory of stress and strain variations in viscous layers, and its geological implications. *Tectonophysics* **72**, 75–103.

Treagus, S. H. 1983. A theory of finite strain variation through contrasting layers, and its bearing on cleavage refraction. *J. Struct. Geol.* **5**, 351–368.

Treagus, S. H. 1988. Strain refraction in layered systems. *J. Struct. Geol.* **10**, 517–527.

Treagus, S. H. & Sokoutis, D. 1992. Laboratory modelling of strain variation across rheological boundaries. *J. Struct. Geol.* **14**, 405–424.

Tsenn, M. C. & Carter, N. L. 1987. Upper limits of power law creep of rocks. *Tectonophysics* **136**, 1–26.

Weijermars, R. & Schmeling, H. 1986. Scaling of Newtonian and non-Newtonian fluid dynamics without inertia for quantitative modelling of rock flow due to gravity (including the concept of rheological similarity). *Phys. Earth & Planet. Interiors* **43**, 316–330.

APPENDIX 1
ALGEBRA FOR PLANE FLOW VARIATIONS

(1) *Requirement of equal* $\dot{e}_{xx}$ *for all layers*. For plane-strain isovolumetric flows, $\dot{e}_{xx}$ can be written as

$$\dot{e}_{xx} = -\dot{e}_1 \cos 2\theta$$

for each layer, where $\dot{e}_1$ is the principal elongating strain rate, at $(\theta - 90)°$ to layering, x is parallel to layering, and y is perpendicular (Fig. 1).

Hence, subscripting with C for competent (stiffer) layers and I for incompetent, throughout,

$$\dot{e}_{1(C)} \cos 2\theta_C = \dot{e}_{1(I)} \cos 2\theta_I = \dot{e}_{1(bulk)} \cos 2\theta_{(bulk)}. \quad (A1)$$

Normalizing the principal flows to factors of the bulk principal flow, as

$$\varepsilon_C = \dot{e}_{1(C)}/\dot{e}_{1(bulk)}, \quad \varepsilon_I = \dot{e}_{1(I)}/\dot{e}_{1(bulk)}, \quad (A2)$$

gives

$$\varepsilon_C = \cos 2\theta/\cos 2\theta_C \quad (A3a)$$

and

$$\varepsilon_I = \cos 2\theta/\cos 2\theta_I. \quad (A3b)$$

(2) *Requirement of equal τ_{xy} at the layer interface boundaries* gives

$$\tau_{xy(C)} = \tau_{xy(I)} = \tau_{xy(bulk)}. \quad (A4)$$

Write in terms of shear viscosity, μ, and strain rate $\dot{e}_{xy}$, as

$$\tau_{xy} = 2\mu\dot{e}_{xy}$$

$$\dot{e}_{xy(C)}/\dot{e}_{xy(I)} = \mu_I/\mu_C.$$

Define the viscosity ratio $\mu_C/\mu_I = M$, and write in terms of principal strain rates

$$\dot{e}_{1(C)} \sin 2\theta_C/\dot{e}_{1(C)} \sin \theta_I = 1/M,$$

or in normalized form

$$\varepsilon_C \sin 2\theta_C/\varepsilon_I \sin 2\theta_I = 1/M. \quad (A5)$$

Substituting (A3) gives

$$\tan 2\theta_C/\tan 2\theta_I = 1/M. \quad (A6)$$

For Newtonian materials, this is equivalent to equation (9) in Treagus (1973).

(3) *The requirement of bulk multilayer strain* is that the sum of individual layer-parallel shear strains, divided by total thickness, is the bulk (or average) shear strain (Biot 1965, p. 432). Using α_C for the competent layer thickness proportion, and α_I for incompetent (where $\alpha_C + \alpha_I = 1$),

$$\dot{e}_{xy(bulk)} = \alpha_C\dot{e}_{xy(C)} + \alpha_I\dot{e}_{xy(I)}.$$

Writing, as before, in terms of normalized principal strain rates gives

$$\varepsilon_C\, \alpha_C \sin 2\theta_C + \varepsilon_I\, \alpha_I \sin 2\theta_I = \sin 2\theta. \quad (A7)$$

Substituting for ε_C and ε_I from (A3) gives

$$\alpha_C \tan 2\theta_C + \alpha_I \tan 2\theta_I = \tan 2\theta. \quad (A8)$$

Then, from (A6),

$$\tan 2\theta_C = \tan 2\theta/(\alpha_C + M\, \alpha_I) \quad (A9a)$$

and

$$\tan 2\theta_I = M \tan 2\theta/(\alpha_C + M\alpha_I). \quad (A9b)$$

For equal thickness layers (i.e. $\alpha_C = \alpha_I = 0.5$),

$$\tan 2\theta_C = 2 \tan 2\theta/(1 + M), \quad (A10a)$$

and

$$\tan 2\theta_I = 2M \tan 2\theta/(1 + M). \quad (A10b)$$

Up to this stage, it is clear that if $\theta = 0°$ or $90°$ (layer-parallel pure shearing, LPPS), $\tau_{xy} = 0$, and so $\varepsilon_C = \varepsilon_I = 1$, which proves homogeneous flow. For $\theta = 45°$ (layer-parallel simple shearing, LPSS), $\dot{e}_{xx} = 0$, (A6) reduces to $\varepsilon_C/\varepsilon_I = 1/M$, and (A7) reduces to $\varepsilon_C\, \alpha_C + \varepsilon_I\, \alpha_I = 1$.

(4) *Determining viscosity ratio*, M. This is a constant, independent of strain orientation and strain rates, only for Newtonian materials ($n = 1$). For $n \neq 1$, M is a variable. The simplified expression used for two-dimensional power-law flow (after Tsenn & Carter 1987), $\dot{e} = A\, \sigma^n$ (where $\dot{e}$ is the steady-state strain rate, σ the differential stress, A a material constant, and n the stress exponent), can be written as $\sigma = 2\,\mu\dot{e}$, with viscosity, μ, given by

$$\mu = \dot{e}^{(1/n-1)}/2A^{1/n} \quad (A11)$$

(Cobbold 1983, equation 59). For a bilaminate multilayer with layers of equal n value, it is found that

$$M = \mu_C/\mu_I = R \cdot [\varepsilon_C/\varepsilon_I]^{1/n-1}, \quad (A12)$$

where $R = (A_I/A_C)^{1/n}$ is the viscosity ratio for layer-parallel pure shearing (Cobbold 1983, equation 62). It was noted in Section (3) that for $\theta = 45°$, $\varepsilon_C/\varepsilon_I = 1/M$, and thus (A12) simplifies to $M = R^n$ (Cobbold 1983, equation 64).

The determination of M for particular values of R, θ, α_C and α_I is achieved as follows. Squaring (A9) and making the trigonometric substitution $1 + \tan^2 2\theta = \sec^2 2\theta$, gives

$$\cos^2 2\theta_C = (\alpha_C + M\alpha_I)^2/[(\alpha_C + M\alpha_I)^2 + \tan^2 2\theta] \quad (A13a)$$

and

$$\cos^2 2\theta_I = (\alpha_C + M\alpha_I)^2/[(\alpha_C + M\alpha_I)^2 + M^2 \tan^2 2\theta]. \quad (A13b)$$

From (A3) squared and (A13),

$$(\varepsilon_I/\varepsilon_C)^2 = [(\alpha_C + M\alpha_I)^2 + M^2 \tan^2 2\theta]/[(\alpha_C + M\alpha_I)^2 + \tan^2 2\theta]. \quad (A14)$$

Using (A12), (A14) becomes

$$(M/R)^{2n/(n-1)} = [(\alpha_C + M\alpha_I)^2 + M^2 \tan^2 2\theta]/[(\alpha_C + M\alpha_I)^2 + \tan^2 2\theta]. \quad (A15)$$

This polynomial can be solved for M in terms of R by keeping only the M^2 right-hand terms. This can be shown to be valid for the cases used in this paper of $R = 10$ (or more), and M always $> R$. However, it also requires $M\alpha_I >> 2\,\alpha_C$, so will break down as α_I approaches zero.

Using this method of solution for M, yields

$$M^{2n/(n-1)} \approx R^{2n/(n-1)}[1 + \tan^2 2\theta/\alpha_I^2],$$

which can be rewritten as

$$M \approx R[1 + (\tan^2 2\theta/\alpha_I^2)]^{(n-1)/2n}. \quad (A16)$$

This is the expression which will be used for M.

For equal thickness layers ($\alpha_C = \alpha_I = 0.5$),

$$M \approx R[1 + 4 \tan^2 2\theta]^{(n-1)/2n}.$$

Recall, from earlier, that equation (A16) will not be valid for $\theta = 45°$, where $M = R^n$, regardless of thicknesses α_C and α_I.

The key equations required for determining values of flow partitioning are summarized from the above algebra, as equations (1)–(3) in the main text.

APPENDIX 2
ALGEBRA FOR THREE-DIMENSIONAL FLOWS

The expression used for two-dimensional power-law flow, $\dot{e} = A\sigma^n$, is a simplification of the general expression for power-law Reiner–Rivlin fluids

$$d = A\, \tau^n,$$

where d is the second invariant of the strain-rate (stretching) tensor

$$d^2 = \tfrac{1}{2}(\dot{e}_1^2 + \dot{e}_2^2 + \dot{e}_3^2) \quad (A17)$$

and τ is the octahedral shear stress (Cobbold 1983). Thus the shear viscosity is

$$\mu = d^{(1/n-1)}/2A^{1/n}. \quad (A18)$$

For isovolumetric plane flow, as considered in Appendix 1, $\dot{e}_2$ is zero; hence $d = \dot{e}_1$, and (A18) is written as (A11). The expressions formerly derived (A1–A16) could thus be written in terms of maximum principal strain rates, $\dot{e}_1$, and normalized values (e.g. ε_C). However, where flow is three-dimensional, and includes flow perpendicular to the plane of view in Fig. 1, the expression for viscosity ratio, M, is in terms of d, and the method of solution of equations satisfying flow compatibility is more involved.

For three-dimensional flow, the viscosity ratio $M = \mu_C/\mu_I$ is written

$$M = \mu_C/\mu_I = R \cdot [d_C/d_I]^{1/n-1}, \quad (A19)$$

where $R = (A_I/A_C)^{1/n}$, as before, and d_C and d_I refer to strain-rate invariants (as A17) in the competent and incompetent layers.

Only the case where flow in the third (z) dimension (perpendicular to the page in Fig. 1c) is a principal strain-rate (parallel to layering) will be considered in this paper. Assume this to be a non-zero $\dot{e}_2$ for the present. (The following maths will allow interchange of principal values so that this third dimension of layer-parallel principal straining can also be $\dot{e}_1$ or $\dot{e}_3$.) This system has been termed "two-dimensionally oblique" (Treagus 1981, 1988).

For isovolumetric flow ($\dot{e}_1 + \dot{e}_2 + \dot{e}_3 = 0$) for the bulk material, and for the competent and incompetent components, d can be written from (A17) in terms of $\dot{e}_1$ and $\dot{e}_2$:

$$d^2 = (\dot{e}_1^2 + \dot{e}_1\dot{e}_2 + \dot{e}_2^2). \quad (A20)$$

As in Appendix 1, it is useful to normalize the principal strain rates in each layer as ratios of bulk $\dot{e}_1$, termed ε (see A2). However, an additional term is needed to express the non-plane nature of the bulk flow. This, termed E, is defined as the normalized layer-parallel flow in the third dimension ($\dot{e}_2$), here $\dot{e}_2$:

$$E = \dot{e}_2/\dot{e}_{1(\text{bulk})}. \tag{A21}$$

Now, from (A19), M can be written as

$$(M/R)^{n/(1-n)} = d_C/d_I, \tag{A22}$$

which becomes from (A20), and for equal $\dot{e}_2$ throughout the multilayer

$$(M/R)^{2n/(1-n)} = (\dot{e}_{1(C)}^2 + \dot{e}_{1(C)}\dot{e}_2 + \dot{e}_2^2)/ (\dot{e}_{1(I)}^2 + \dot{e}_{1(I)}\dot{e}_2 + \dot{e}_2^2). \tag{A23}$$

So writing in terms of normalized flows ε_C, ε_I and E

$$(M/R)^{2n/(1-n)} = (\varepsilon_C^2 + \varepsilon_C E + E^2)/(\varepsilon_I^2 + \varepsilon_I E + E^2). \tag{A24}$$

This is a more complex expression than its equivalent (A12) for plane flow.

(1) *Requirement of equal* $\dot{e}_{xx}$ *in all layers* is written for non-plane flows in the form

$$\dot{e}_{xx} = \tfrac{1}{2}[(\dot{e}_1 + \dot{e}_3) - (\dot{e}_1 - \dot{e}_3)\cos 2\theta],$$

which, when equated (cf. A1) for competent, incompetent and bulk relationships, and following the above normalizations gives

$$(2\varepsilon_C + E)\cos 2\theta_C = (2\varepsilon_I + E)\cos 2\theta_I = (2 + E)\cos 2\theta. \tag{A25}$$

So

$$\varepsilon_C = \tfrac{1}{2}[(2 + E)\cos 2\theta/\cos 2\theta_C - E] \tag{A26a}$$

$$\varepsilon_I = \tfrac{1}{2}[(2 + E)\cos 2\theta/\cos 2\theta_I - E]. \tag{A26b}$$

(2) *Requirement of equal* τ_{xy} *at the layer interface boundaries* means

$$\dot{e}_{xy(C)}/\dot{e}_{xy(I)} = \mu_I/\mu_C = 1/M.$$

In the present case, and written, as above, in normalized form

$$(2\varepsilon_C + E)\sin 2\theta_C/(2\varepsilon_I + E)\sin 2\theta_I = 1/M. \tag{A27}$$

From (A25) it follows

$$\tan 2\theta_C/\tan 2\theta_I = 1/M \tag{A28}$$

as for plane flows (A7).

(3) *Requirements of bulk multilayer strain* are

$$\alpha_C(2\varepsilon_C + E)\sin 2\theta_C + \alpha_I(2\varepsilon_I + E)\sin 2\theta_I = (2 + E)\sin 2\theta. \tag{A29}$$

From (A25),

$$\alpha_C\tan 2\theta_C + \alpha_I \tan 2\theta_I = \tan 2\theta \tag{A30}$$

$$\tan 2\theta_C = \tan 2\theta/(\alpha_C + M\alpha_I) \tag{A31a}$$

$$\tan 2\theta_I = M \tan 2\theta/(\alpha_C + M\,\alpha_I). \tag{A31b}$$

These are equivalent to (A8) and (A9) in Appendix 1.

(4) *Determination of* M involves squaring (A25) and rearranging to

$$\cos^2 2\theta_C = (2 + E)^2 \cos^2 2\theta/(2\varepsilon_C + E)^2 \tag{A32a}$$

$$\cos^2 2\theta_I = (2 + E)^2 \cos^2\ 2\theta/(2\varepsilon_I + E)^2. \tag{A32b}$$

Squaring (A31) and making trigonometric substitutions, as in Appendix 1, gives

$$\cos^2 2\theta_C = (\alpha_C + M\alpha_I)^2/[(\alpha_C + M\alpha_I)^2 + \tan^2 2\theta]. \tag{A33a}$$

$$\cos^2 2\theta_I = (\alpha_C + M\alpha_I^2)^2/[(\alpha_C + M\alpha_I)^2 + M\tan^2 2\theta]. \tag{A33b}$$

Equating (A32) and (A33), and writing

$$B = \alpha_C + M\alpha_I \tag{A34}$$

yields

$$(2\varepsilon_C + E)^2 = (2 + E)^2 \cos^2 2\theta\,(B^2 + \tan^2 2\theta)/B^2 \tag{A35a}$$

$$(2\varepsilon_I + E)^2 = (2 + E)^2 \cos^2 2\theta\,(B^2 + M\tan^2 2\theta)/B^2. \tag{A35b}$$

These expressions must be solved with (A24), to determine M, so they need to be expressed in terms of $(\varepsilon_C^2 + \varepsilon_C E + E^2)$ and $(\varepsilon_I^2 + \varepsilon_I E + E^2)$. Noting

$$4(\varepsilon_C^2 + \varepsilon_C E + E^2) = (2\varepsilon_C + E)^2 + 3E^2$$

(A24) is rewritten

$$(M/R)^{2n/(1-n)} = [(2 + E)^2(B^2\cos^2 2\theta + \sin^2 2\theta) + 3B^2E^2]/ [(2 + E)^2(B^2\cos^2 2\theta + M^2\sin^2 2\theta) + 3B^2E^2]. \tag{A36}$$

Expanding B (from A34), and just including M^2 terms to allow a solution for M in terms of R to be obtained (as Appendix 1), gives

$$M \approx R[1 + \sin^2 2\theta/\{\alpha_I^2(\cos^2 2\theta + 3F)\}]^{(n-1)/2n}, \tag{A37}$$

where

$$F = E^2/(2 + E)^2. \tag{A38}$$

This is the key equation for M in non-plane flows.

At very high n, $\{(n - 1)/2n\} \to 1/2$, and so (A37) tends to

$$M \approx R\sqrt{[1 + \sin^2 2\theta/\{\alpha_I^2(\cos^2 2\theta + 3F)\}]}.$$

For plane flows, $E = 0$, so $F = 0$, and (A37) becomes equivalent to (A16).

For pure flattening bulk flow, $E = 1$, and thus $F = 1/9$. For pure constrictional bulk flow, $E = -1/2$, and $F = 1/9$, also. So these two cases have identical M expressions (A37), for the same R, α_I and θ. For equal-thickness layers ($\alpha_I = 0.5$) in pure bulk flattening or constriction,

$$M \approx R[1 + 12\sin^2 2\theta/(3\cos^2 2\theta + 1)]^{(n-1)2n}. \tag{A39}$$

For $\theta = 45°$, this becomes

$$M \approx R(13)^{(n-1)/2n}. \tag{A40}$$